Mon. Not. R. Astron. Soc. **000**, 1–10 (2012) Printed 2 March 2013 (MN LATEX style file v2.2)

Millimeter and sub-millimeter atmospheric performance at Dome C combining radiosoundings and ATM synthetic spectra

S. De Gregori,[1⋆] M. De Petris,[1] B. Decina,[1] L. Lamagna,[1] J. R. Pardo,[2] B. Petkov,[3] C. Tomasi,[3] L. Valenziano,[4]
[1] *Department of Physics, Sapienza University of Rome, Italy*
[2] *Centro de Astrobiologa (CSIC/INTA), Instituto Nacional de Técnica Aeroespacial, Madrid, Spain*
[3] *Institute of Atmospheric Sciences and Climate, Consiglio Nazionale delle Ricerche, Bologna, Italy*
[4] *Institute of Space Astrophysics and Cosmic Physics, National Institute for Astrophysics, Bologna, Italy*

Received 2012 May 3; accepted 2012 May 31

ABSTRACT
The reliability of astronomical observations at millimeter and sub-millimeter wavelengths closely depends on a low vertical content of water vapour as well as on high atmospheric emission stability. Although Concordia station at Dome C (Antarctica) enjoys good observing conditions in this atmospheric spectral windows, as shown by preliminary site-testing campaigns at different bands and in, not always, time overlapped periods, a dedicated instrument able to continuously determine atmospheric performance for a wide spectral range is not yet planned. In the absence of such measurements, in this paper we suggest a semi-empirical approach to perform an analysis of atmospheric transmission and emission at Dome C to compare the performance for 7 photometric bands ranging from 100 GHz to 2 THz. Radiosoundings data provided by the Routine Meteorological Observations (RMO) Research Project at Concordia station are corrected by temperature and humidity errors and dry biases and then employed to feed ATM (Atmospheric Transmission at Microwaves) code to generate synthetic spectra in the wide spectral range from 100 GHz to 2 THz. This approach is attempted for the 2005-2007 dataset in order to check its feasibility. To quantify the atmospheric contribution in millimeter and sub-millimeter observations we are considering several photometric bands, largely explored by ground based telescopes, in which atmospheric quantities are integrated. The observational capabilities of this site at all the selected spectral bands are analyzed considering monthly averaged transmissions joined to the corresponding fluctuations. Transmission and *pwv* statistics at Dome C derived by our semi-empirical approach are consistent with previous works. It is evident the decreasing of the performance at high frequencies. We propose to introduce a new parameter to compare the quality of a site at different spectral bands, in terms of high transmission and emission stability, the Site Photometric Quality Ratio. The effect of the instrument filter bandwidth is involved on the estimate of the optical depth performed by the water vapour content knowledge.

Key words: Site testing – Atmospheric effects – Submillimetre – Cosmology: observations.

1 INTRODUCTION

Astronomy and astrophysics in the 100-1000 GHz band allow the study of a large variety of processes, in the local and distant universe, which involve cool matter absorbing and reradiating efficiently at these frequencies, in environments often unaccessed through observations at visible wavelengths. In fact, many key topics in modern astronomy and cosmology, such as galaxy formation and evolution, the amount and role of dark matter and dark energy in the universe, star formation, protoplanetary disks, or the properties of cold debris at the outskirts of the solar system, are related to radiative phenomena in this band. The field has undergone a huge development in the last two decades, thanks to the de-

⋆ E-mail: simone.degregori@roma1.infn.it

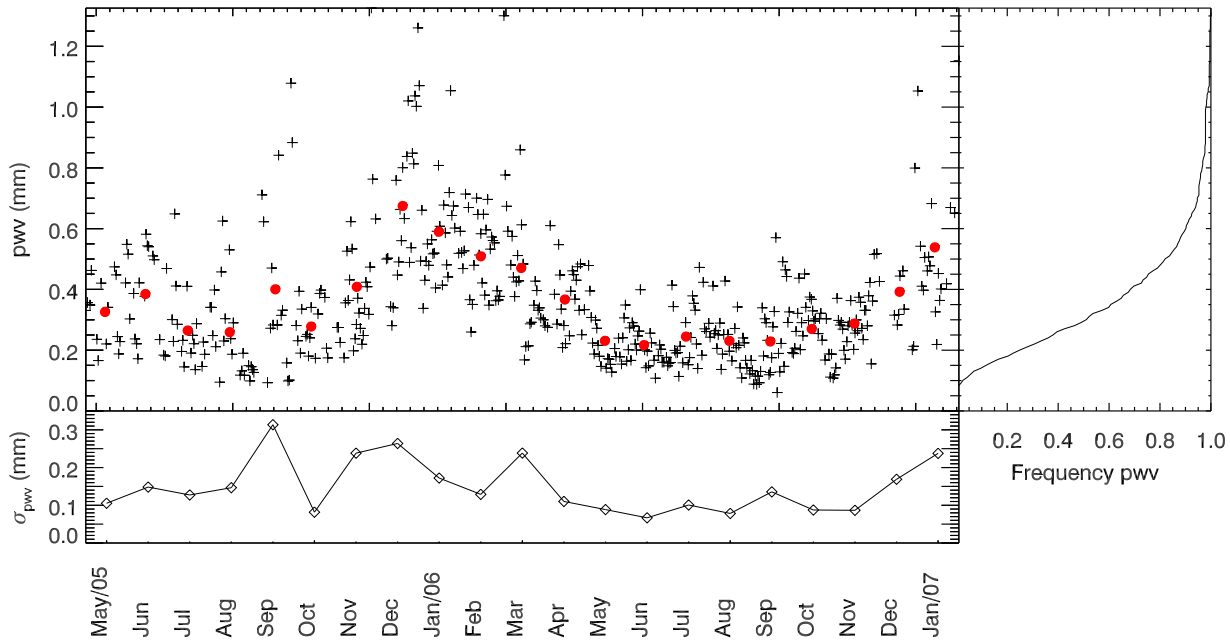

Figure 1. Daily values of precipitable water vapour (*pwv*) estimated from the 12:00 UTC radiosounding measurements performed at Dome C over the period from May 2005 to January 2007 are shown in the upper left panel. Monthly averages of *pwv* are overplotted as red dots. In the right panel the corresponding *pwv* vs. cumulative frequency is plotted. The bottom panel shows the monthly *pwv* fluctuations quantified as the daily values standard deviation, σ_{pwv}.

velopment of sensitive detectors, large cameras, polarization sensitive devices and spectroscopically capable instrumentation. Some key achievements range from the measurement of the intensity and polarization power spectra of the cosmic microwave background at millimeter (mm) wavelengths, to the discovery and the characterization of the optically elusive sub-millimeter (sub-mm) galaxy population (SCUBA, BLAST), and the recent galaxy cluster surveys through sub-arcminute resolution observations of the Sunyaev-Zel'dovich effect (ACT, SPT).

Ground-based observations in the mm/sub-mm band are usually plagued by the transparency of the atmosphere (and its stability over time), mainly because of the presence of large, time-dependent pressure-broadened features in the emission (and absorption) spectrum of the water vapour. Of course, this issue is strongly mitigated when operating stratospheric balloon-borne or airborne detectors, and completely averted when moving detectors on spacecrafts. BOOMERANG, BLAST, SOFIA, *Planck* and *Herschel* have proven the effectiveness of mm and sub-mm observations from the stratosphere and from space, providing ground breaking advancements in their respective fields at the time of their operation.

Anyway, the practical limitations on the telescope size, the weight and the accessibility of instrumentation still make substantially unfeasible the deployment of large (10m class) telescopes on balloons, aircrafts or satellites. As a matter of fact, the ground-based solution appears presently the only viable way to routinely perform high angular resolution observations of compact objects and/or small spatial and spectral features in cool diffuse media at sub-mm wavelengths.

As a consequence, the last few years have witnessed increasing efforts in the design and construction of large telescopes in places of the planet which provide the potentially most attractive atmospheric features for mm and sub-mm astronomy. The community has realized the need to perform a thorough characterization of astronomical sites in terms of atmospheric opacity and stability across the whole mm/sub-mm spectral region, both for observation planning and for transparency monitoring during the observing sessions.

At a time where bolometric detectors can easily approach the photon noise limit, and large cameras with hundreds or thousands of such detectors already allow to break this limitation, it is straightforward to realize that an improper characterization of the atmospheric properties may become the strongest restriction to the effective science return from ground-based instruments of the present (ACT, SPT) and next generation (CCAT).

In order to continuously monitor the atmospheric transmission several approaches are possible: tippers or tau-meters, hygrometers, GPS, water vapour radiometers, radiosoundings and spectrometers. The first approaches allow a continuous data recording by simple instruments but with the drawback of single frequency observations, needing a synthetic atmospheric model to infer transmission at other frequencies.

Dome C is considered one of the best sites in the world to perform observations in a wide range of the electromagnetic spectrum allowing also to explore Terahertz windows (Minier et al. (2008) and Tremblin et al. (2011)). Anyway a wide frequency coverage transmission measurements campaign at Dome C, employing the direct spectroscopic information derived by an interferometric experiment, was never carried out.

The goal of this paper is to compensate the lack of those data by estimating the atmospheric performance with a semi-empirical approach. We test this method using the available dataset of radiosounding measurements recorded by

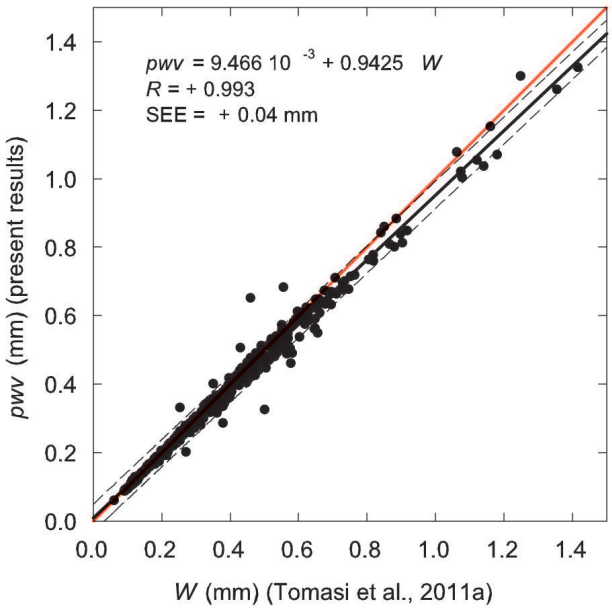

Figure 2. Daily values of precipitable water vapour (pwv) obtained through the present analysis from surface-level to 8 km amsl, and plotted versus W, the corresponding values of precipitable water derived by Tomasi et al. (2011a) over the altitude range from surface-level to 12 km amsl. The data are best-fitted by a regression line with intercept equal to 9.46610^{-3} and slope coefficient equal to 0.9425, which was obtained with regression coefficient R = +0.993, and provided a standard error of estimate SEE = 0.04 mm.

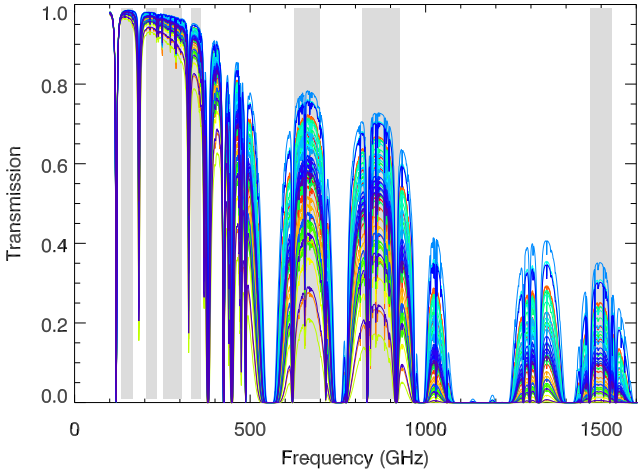

Figure 3. Atmospheric transmission spectra as modeled by ATM program for each radiosounding. Photometric bands in Table 1 (gray) match the main transmission windows.

Table 1. Characteristic spectral bands assumed in this work.

	ν_0 (GHz)	λ_0 (μm)	FWHM(%)	References
LF	150	2000	22	1, 2, 3, 4
	220	1400	13	1, 2, 3
	270	1100	18	1, 2, 3
	350	860	8	1, 2, 5, 6
HF	660	450	11	5, 6
	870	350	13	5
	1500	200	5	7

References: (1) SPT, Schaffer et al. (2011); (2) MITO, De Petris et al. (2002); (3) ACT, Swetz et al. (2011); (4) BRAIN, Battistelli et al. (2012); (5) SCUBA, Holland et al. (1999); (6) SCUBA-2, Dempsey et al. (2010); (7) THUMPER, Ward-Thompson et al. (2005);

the Routine Meteorological Observations (RMO) Research Project (www.climantartide.it) at Concordia station in the period from May 2005 to January 2007, carefully corrected for the main lag errors and dry biases. The profiles of air temperature, pressure and relative humidity allow to generate synthetic spectra, ranging from 100 GHz to 2 THz, with the ATM code (Pardo et al. (2001a)).

The paper is organized as follows. Atmospheric synthetic spectra, as derived by ATM code, are described in Sect. 2.

In Sect. 3 estimates of atmospheric transmission and emission corresponding to largely explored ground based telescope bands between 150 and 1500 GHz are analyzed. The effect of the filter bandwidths on the estimate of opacity is for the first time included in the relation showing a contribution up to a 30 per cent over-estimate on the opacity in the case of the highest frequency band.

A parameter to rank the observational conditions for each of the selected spectral bands is introduced as the ratio between average transmission and the corresponding fluctuations.

Finally a discussion on the analysis and the conclusions are summarized in Sect. 4.

A detailed description of the correction procedure used to analyse the raw radiosounding data and determine the vertical profiles of the main thermodynamic parameters is reported in the Appendix.

2 SYNTHETIC SPECTRA PRODUCTION

At present, for the site of Dome C we can rely only on the atmospheric monitoring performed at a few individual frequencies, with no simultaneous measurements in different regions of the spectrum. In order to compensate for the lack of a continuous and spectrally wide atmospheric monitoring at Dome C, we predict the performance in the mm/sub-mm bands in the period from May 2005 to January 2007 by means of a semi-empirical approach.

A set of raw radiosounding data was recorded for the present study, consisting of an overall number of 469 radiosounding measurements taken routinely at Dome C, at 12:00 UTC from May 2, 2005 to January 31, 2007 ranging from a minimum of 15 in May 2005 to a maximum of 30 in November 2006.

In general, each radiosonde measurement consists of values of air pressure P, air temperature T and relative humidity RH, taken at more than 800 standard and additional levels in the altitude range from surface to 10 km above mean sea level (amsl). Data provided by the radiosonde sensors are affected by lag and instrumental errors as well as by various dry biases. They were all corrected following the procedure

described in the Appendix.
The time-patterns of the daily *pwv* values are shown in Fig. 1. Two main features are evident in Fig. 1, showing that the majority of *pwv* values are lower than 0.3 mm during the austral autumn months, although presenting largely dispersed patterns (of 50 per cent or more), and, hence, low stability.
As shown by Tomasi et al. (2011a), a limited contribution is given to the overall value of atmospheric *pwv* by the amount of water vapour present in the Upper Troposphere and Low Stratosphere (UTLS) region from 8 to 12 km amsl, while negligible fractions of *pwv* ranging mainly between 0.003 and 0.005 mm throughout the year are present in the stratosphere from 12 to 50 km above Dome C (Tomasi et al. (2011b)).
To verify the reliability of the present estimates of *pwv*, a comparison is made in Fig. 2 among the present daily values of *pwv* and those correspondingly determined by Tomasi et al. (2011a) (indicated as W) using a more advanced correction procedure from surface-level to 12 km amsl. The comparison showed that a close relationship exists between the present results and those of Tomasi et al. (2011a), defined by a regression line with nearly null intercept and slope coefficient of + 0.9425, having regression coefficient better than + 0.99, and providing a standard error of estimate equal to 0.04 mm. These findings clearly indicate that the present evaluations of *pwv*, as obtained over the altitude range from surface-level to 8 km amsl, are fully suitable for the purposes of our study, especially considering the intrinsic uncertainty of the simulation model.

We have estimated synthetic spectra in emission and in opacity by means of the ATM code in the wide spectral range from 100 GHz to 2 THz. Each spectrum is derived considering the corrected radiosounding data. The transmission corresponding to each radiosounding dataset, estimated from optical depth spectra as $T = e^{-\tau}$, is shown in Fig. 3.
In the period under consideration, the inferred *pwv* values show an average close to 0.3 mm with a mean dispersion of about 150 μm (see Fig. 1). The same amount of *pwv* variation can contribute with a different weight to the total optical depth. As example in Fig. 4 we represent the optical depth fluctuations derived by ATM, quantified as the maximum dispersion, due to fluctuations of *pwv* of the order of 150 μm around three different *pwv* values (0.15, 0.5 and 1.0 mm). It is worthy of note that for low *pwv* content, $\Delta\tau$ can be as high as 60 per cent in the high frequency windows.

3 MULTI-BAND ANALYSIS

A quantitative analysis is performed considering 7 photometric bands centered at the frequencies of several astrophysical and cosmological experiments: South Pole Telescope (SPT), Atacama Cosmology Telescope (ACT), Millimetre and Infrared Testagrigia Observatory (MITO) and BRAIN (B-mode RAdiation INterferometer) for Low Frequency (LF) atmospheric windows; Submillimetre Common-User Bolometer Array (SCUBA and SCUBA-2) and Two HUndred Micron PhotometER (THUMPER) for sub-mm bands (High Frequency, HF). The central frequency of each

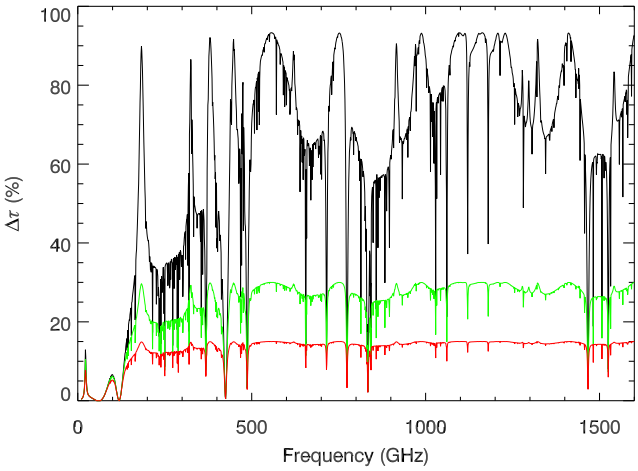

Figure 4. Optical depth fluctuations corresponding to a 150 μm variation around three selected *pwv* values: 1 mm (red line), 500 μm (green line), 150 μm (black line).

band, as well as the bandwidth, quantified with the FWHM (Full Width Half Maximum), are listed in Table 1 (see also Fig. 3). The band profiles are assumed to be top-hat assuming in this way the maximum rejection to off-band contributions.

To assess the constraints on astronomical observations arising from the atmosphere emission above Dome C, we give an estimate of the NEP (Noise Equivalent Power) and the $NEFD$ (Noise Equivalent Flux Density) for all the seven bands. In fact in such a wide spectral region both the quantities are normally employed: the power density, mainly for the low frequency bands, while the flux density, for the high frequency region. The quoted NEP is the root of the sum of NEP^2_{atm}, the term considering the atmospheric emission fluctuations, and NEP^2_{tele}, i.e. the instrumental contribution to the photon noise. The atmospheric emissivity spectra are generated by ATM. The telescope is assumed a 10-m in diameter Al-mirror with a surface emissivity of the order 3 per cent at 150 GHz and depending on the frequency as $\sqrt{\nu}$. The throughput of the telescope is assumed diffraction limited at each band. Focal plane optical efficiencies are taken as unitary for all the bands as well as telescope main beam efficiency. The dominant sky sources (CMB and dust) are not included, the instrument detector noise is assumed lower than the background noise and the spillover emission is neglected. In order to quantify the maximum variation of these quantities we plot in Fig. 5 NEP and $NEFD$ values for all the bands, for the extreme conditions occurred during the austral summers and winters at Dome C in the 2005-2007 period.

3.1 Dome C statistics comparison

To validate the proposed semi-empirical approach, we compare the derived atmospheric performance with the results available in literature.
Fig. 6 shows Dome C atmospheric transmission as a function of the cumulative time frequency derived by radiosounding data and ATM model for the bands listed in Table 1 (the corresponding quartiles are reported in Table 2). Transmission statistics at Dome C per-

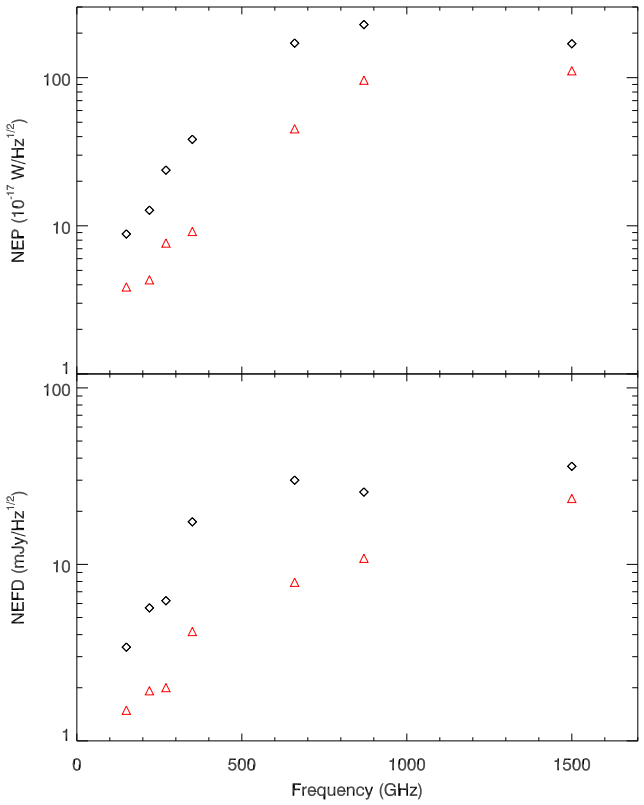

Figure 5. Noise Equivalent Power (upper panel) for the seven bands in two extreme atmospheric conditions in the austral winter (red triangles) and summer (black diamonds). In the lower panel, the same for the Noise Equivalent Flux Density.

Table 2. Transmission quartiles matching cumulative distributions in Fig. 6.

	ν_0 (GHz)	λ_0 (μm)	25%	50%	75%
LF	150	2000	0.97	0.97	0.96
	220	1400	0.95	0.94	0.94
	270	1100	0.94	0.93	0.92
	350	860	0.91	0.89	0.87
HF	660	450	0.64	0.56	0.46
	870	350	0.58	0.50	0.40
	1500	200	0.15	0.08	0.03

Table 3. Pwv quartiles comparison.

Period	25%	50%	75%	References
01/1997	0.38	0.52	0.68	1
05/2005-01/2007	0.20	0.30	0.45	2
2008	0.15	0.24	...	3
2008-2010	0.21	0.27	0.35	4
12/2009-01/2010	0.49	0.75	1.1	5

References: (1) Valenziano & Dall'Oglio (1999); (2) this work; (3) Yang et al. (2010); (4) Tremblin et al. (2011); (5) Battistelli et al. (2012).

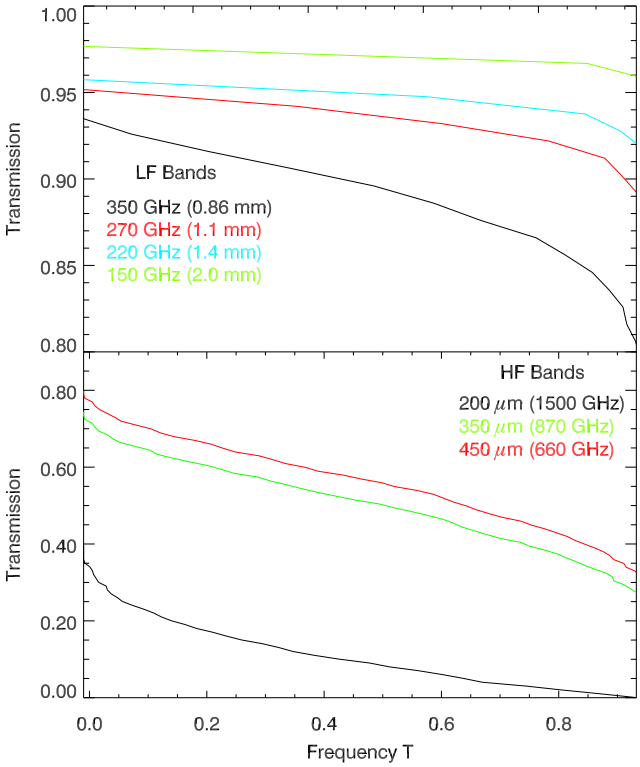

Figure 6. Atmospheric transmission vs. cumulative time frequency for Dome C corresponding to the atmospheric windows listed in Table 1.

formed by Valenziano & Dall'Oglio (1999), Minier et al. (2008), Yang et al. (2010), Tremblin et al. (2011) and Battistelli et al. (2012) are compared with our analysis.

Low frequency atmospheric windows show high transparency during the whole period confirming that high quality mm observations can be performed from this site for most of the time. For instance the 150 GHz 50 per cent quartile transmission is about 97 per cent (see the green line in Fig. 6). This is consistent with the 95 per cent value recently measured by Battistelli et al. (2012) during the summer campaign in December 2009/January 2010, even considering their integrated in-band result.

Median transparency for the 220 GHz atmospheric window is about 95 per cent (see the cyan line in Fig. 6) as already derived by Valenziano & Dall'Oglio (1999) by *pwv* measurements performed with a portable photometer in January 1997.

Dome C 450 μm window remains above a transmission of 60 per cent for 50 per cent of the time. In Minier et al. (2008) the atmospheric transmission at Dome C has been calculated through the 5-years *pwv* data from the South Pole available in Peterson et al. (2003) and extrapolating the corresponding atmospheric transmission at Dome C using the model in Lawrence (2004). They found that 450 μm median transmission at Dome C is about 70 per cent. Recently Yang et al. (2010) measured a 450 μm median winter transmission at Dome C of about 60 per cent estimating *pwv* with the Microwave Humidity Sounder (MHS) sounding on the National Oceanic and Atmospheric Administration (NOAA) ozonesondeas in 2008.

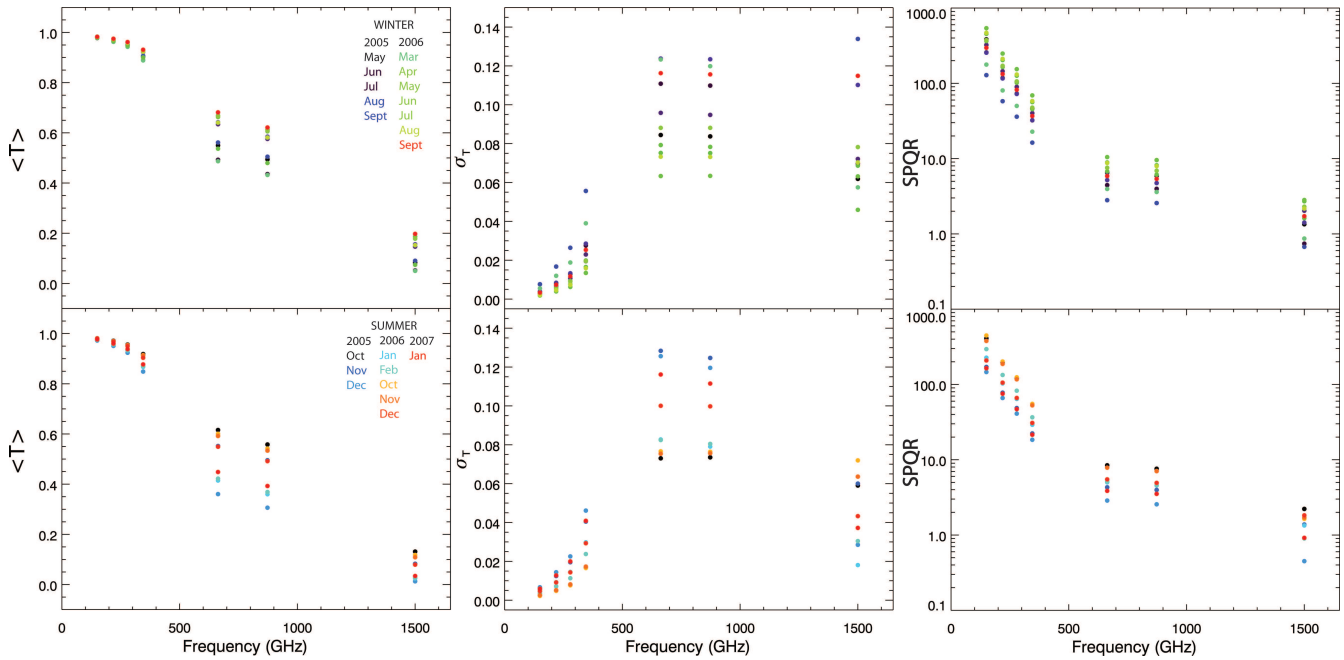

Figure 7. Monthly average values of transmission $\langle T \rangle$ and the relative monthly fluctuations σ_T, plotted as rms values, shown in different colors: austral winter months in the upper panel and summer months in the bottom panel. Monthly Site Photometric Quality Ratio (SPQR) values are shown in the right panel.

Dome C median transmission for the 350 μm atmospheric window is about 50 per cent (see the bottom panel in Fig. 6), as derived by Tremblin et al. (2011) using the MOLIERE model and 200 μm optical depth measurements. They found also that the Dome C 200 μm window opens with a transmission of 10 per cent for less then 25 per cent of the time while Yang et al. (2010) found that the transmission at 200 μm is about 13 per cent for 25 per cent of the time in 2008.
The 200 μm transmission as a function of the cumulative frequency is the black solid line in the bottom panel of Fig.6: the 25 per cent quartile transmission value is above 10 per cent.
Pwv quartiles since May 2005 until January 2007 (see the right panel in Fig. 1) have been compared with Dome C water vapour estimates performed in previous works in Table 3.

3.2 High transmission and emission stability

Following an observational approach, we report the statistics of integrated in-band quantities, like emission and transmission. Both monthly averages $\langle T \rangle$ and relative dispersions σ_T (*rms* values) of in-band transmissions, ranging from May 2005 until January 2007 and splitting between austral summer (from October to February) and winter months (from March to September) are shown in Fig. 7.

Monthly averaged transmission fluctuation is a good proxy of emission stability due to the fact that transmission and emission fluctuations are linearly correlated. In addition we assume that the estimated monthly averaged fluctuations, quantified in terms of the standard deviation, could be an underestimate of atmospheric stability because they derive from a daily data sampling, the time interval between two consecutive radiosoundings.
We note that during the austral winter the atmospheric transmission in all the considered bands is generally higher, as expected. $\langle T \rangle$ shows values close to the unity in mm bands and decreases towards THz windows, while relative dispersions σ_T have the opposite trend. As an example, the best atmospheric conditions (in term of high transmission) occur when the atmospheric fluctuations σ_T are larger than others months (red dots in Fig. 7). Referring to the atmospheric window centered at 200 μm, when the transmission has the maximum value, the large fluctuations at short time scales are likely to degrade the quality of a scientific observation. In addition it is not possible to identify the month with the best atmospheric performance as one can see from the gap between two consecutive years atmospheric transmission and fluctuations (red and blue dots in Fig. 7).
450μm and 350μm bands transmission show a reduction of few percent ranging from winter to summer months, while fluctuations are not sensitive to seasonal effects.
All the considered bands are characterized by high stability

Table 4. Seasonal averages of the SPQR.

	ν_0 (GHz)	Summer	Winter
LF	150	272	335
	220	127	152
	270	79	94
	350	36	42
HF	660	6	7
	870	5	6
	1500	1	2

in October (see the black or orange dots in the middle panel of Fig. 7) with the exception of the 200 μm window, showing high stability especially during summer months like January or February, when atmospheric transparency is not suitable to perform astrophysical observations.
To quantify the real capability of the observational site we need to study the atmospheric performance, mainly the stability, strongly affected by the weak reproducibility of weather conditions at long time scales. In order to highlight this issue we introduce a specific parameter, the Site Photometric Quality Ratio:

$$SPQR = \frac{\langle T \rangle}{\sigma_T} \quad (1)$$

relating monthly averaged transmission to its fluctuations, sampled on a daily timescale, for all the considered atmospheric windows. SPQR amplitude provides information about atmospheric performance and it allows us to dermine if high transmission combined with high transmission (i.e. emission) stability conditions are both satisfied for each band. Even if we are not able to identify the desired SPQR threshold, this factor could represent a useful tool to compare several bands performance or sites. In the right panel of Fig. 7 monthly values of the Site Photometric Quality Ratio are shown in different colors. The differences between the two years are more evident in SPQR, anyway a decrement of the Site Photometric Quality Ratio towards THz regime occurs in austral winter as well as in summer periods. Seasonal averaged values of the Site Photometric Quality Ratio in Table 4 suggest the good quality of atmospheric conditions in the low frequency bands, notably during the austral winter. While SPQR appears useful for comparison among different bands at Dome C it could also be employed for comparison among different sites. It is worth reminding that it is difficult to quantify for SPQR a threshold value to discriminate the goodness of a site.
Two outcomes can be gathered from this analysis. If we believe in the transmission values, as derived by this semi-empirical approach, a continuous atmospheric sampling is mandatory at least at high frequency to contrast the low transmission stability. Otherwise if we consider the data derived in this work not reliable enough for an accurate estimate of atmospheric properties, we need direct observational techniques. In either case continuous atmospheric transparency measurements in all the spectral range of interest are necessary.

3.3 Effect of broadband filter on optical depth estimate

The average of the optical depth over a band, $\tau_{\nu_0}(\Delta\nu)$, is larger than its central value τ_{ν_0} so the opacity is overestimated by broadband instruments like tippers, as remarked as example by Calisse et al. (2004). The determination of this effect is not unique because several *pwv* values could give the same in-band integrated opacity. Low-frequency instruments are less sensitive to this degeneracy even for large values of the bandwidth due to the flatness of the corresponding atmospheric windows. On the other hand a sub-mm broadband instrument overestimates the opacity (underestimates the transmission) and this difference depends

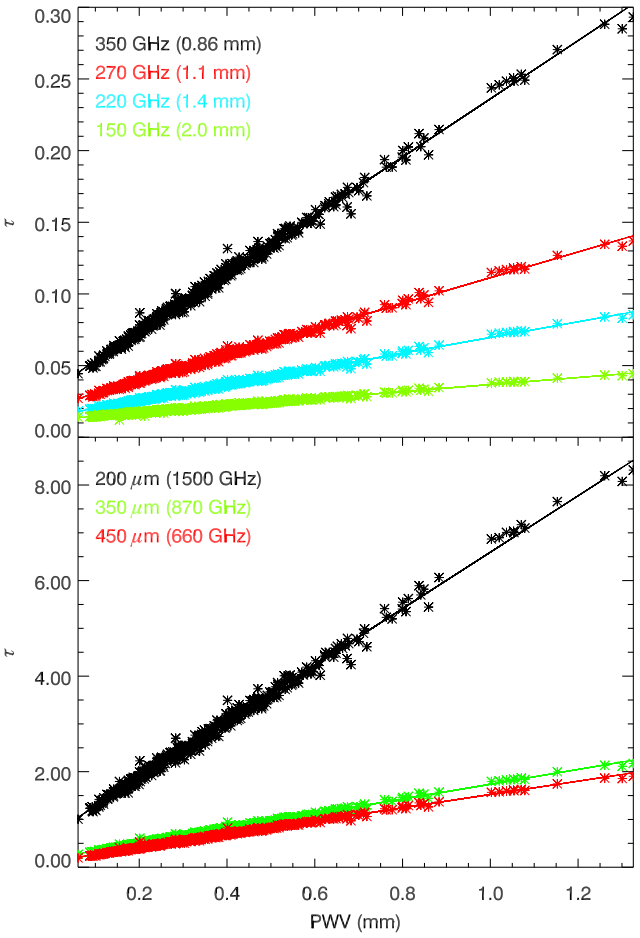

Figure 8. Best fit of the correlation between the narrow-band opacity data and atmospheric water vapour for mm windows (top panel) and for the sub-mm bands (bottom panel).

on the filter shape as well as on the the atmospheric conditions. Little variations of atmospheric conditions give rise to a dispersion of this overestimate because of the relative shapes of the atmospheric window and the corresponding filter. For each band in Table 1 we have included the effect in the relation between the integrated zenith opacity $\tau_{\nu_0}(\Delta\nu)$ and *pwv* values the effect of the instrumental bandwidth $\Delta\nu$ (see Fig. 8 and Table 5):

$$\tau_{\nu_0}(\Delta\nu) = (a_0 + a_1\Delta\nu) + (b_0 + b_1\Delta\nu)pwv \quad (2)$$

a_0 and b_0 are the linear fit coefficients of the $\tau_{\nu 0}$ vs *pwv* relation referred to a narrow band filter matched to the central frequency and a_1 and b_1 take into account the dependency on the instrumental bandwidth $\Delta\nu$, linearly approximated at least in the range within the maximum bandwidths as reported in Table 1. Realistic band profiles could highlight the effect instead of our approximation with top-hat profiles. The net result is that the optical depth can be overestimated at most of 30 per cent at 200 μm, assuming the *pwv* best quartile from Table 3, while low frequency windows are less sensitive to this effect, as expected (10 per cent at 150 GHz).
The uncertainty related to the optical depth value due to the intrinsic scatter of the τ_0 vs *pwv* relation, can be approxi-

Table 5. Opacity-*pwv* relation best fit parameters evaluated for the bands of interest.

	ν_0 (GHz)	a_0	a_1	$b_0(\mathrm{mm}^{-1})$	b_1	c_0	c_1
	150	0.012	0.0077	0.024	0.0054	0.0016	0.0012
LF	220	0.015	0.052	0.053	0.030	0.0024	0.0012
	270	0.024	0.016	0.088	0.0070	0.0040	0.0016
	360	0.032	0.073	0.19	0.41	0.0093	0.014
	660	0.16	0.021	1.35	1.71	0.066	0.073
HF	870	0.18	0.68	1.51	1.96	0.074	0.070
	1500	0.53	10.13	5.82	12.69	0.29	0.35

mated by a linear trend as a function of the instrumental bandwidth:

$$\sigma_{\tau_{\nu_0}}(\Delta\nu) = c_0 + c_1\Delta\nu \quad (3)$$

The optical depth uncertainty turns out to be 0.002 at 150 GHz and rise up to 0.3 at 200 μm, assuming the dispersion independent on *pwv* value (see Fig. 8). As a consequence the percentage uncertainty on optical depth estimate is about 15 per cent all over the considered atmospheric windows assuming the best *pwv* quartile and it remains above 10 per cent even assuming the 75 per cent quartile in Table 3.

The six parameters corresponding to the seven bands are listed in Table 5. The Eq. 2 is useful to infer the atmospheric opacity at the preferred frequency, with a specific bandwidth, when the *pwv* content is known, but it is important to remind that this relation is appropriate only in the environs of Dome C.

In Tremblin et al. (2011) the opacity is related to the atmospheric *pwv* by means of the MOLIERE model. The resulting linear regression of the *pwv* as a function of the 200 μm opacity and the corresponding best fit parameters in Table 5, neglecting a_1 and b_1, gives less than 5 per cent difference in transmission for low *pwv* values. Such a gap could be easily included in the atmospheric performance variations observed at Dome C over the years. Also the difference in transmission evaluated for 220 GHz best fit parameters in Table 5 and $\tau_0(225GHz)$-*pwv* linear fit in Valenziano & Dall'Oglio (1999) is lower then 4 per cent.

4 CONCLUSIONS

The quality of cosmological and astrophysical measurements performed from ground based observational sites in the mm and sub-mm wavelength regions are strongly dictated by the atmospheric performance.

The simultaneous measurement of atmospheric transparency and transmission fluctuations, i.e. emission stability, is a necessary condition to determine the true capabilities of the site of interest.

We try to monitor the atmosphere across a wide spectral range, mm and sub-mm, with a semi-empirical approach. The transmission at Dome C is inferred by generating ATM synthetic spectra as derived by radiosounding data in the period from May 2005 to January 2007. Excellent performance is evident in the low frequency bands while large emission fluctuations are present in the high frequency bands. In fact even if the median winter transmission is large in all the considered atmospheric windows, daily atmospheric emission fluctuations are not negligible and become remarkable in the sub-mm range. In addition, large timescales fluctuations of the atmospheric performance have been detected during two consecutive years.

The ratio between monthly averaged transmission and the corresponding fluctuations, defined Site Photometric Quality Ratio, turns out to be an efficient estimator to rank the photometric performance of the atmosphere, in terms of stability, above Dome C, as well as any observational site. It allows to verify when high transmission as well as low skynoise requirements are satisfied for the atmospheric window of interest. The SPQR threshold for each band is not easily defined: it is depending on the detectors architecture and on the adopted observational strategy.

We attempted to validate the proposed semi-empirical approach comparing *pwv* and transmission quartiles with other site-testing campaigns performed at Dome C during the last years also at different wavelengths.

In the usual linearly dependent opacity-*pwv* relation, we include the effect due to the bandwidth of the monitor instrument.

Anyway only direct and frequent measurements of atmospheric transmission in a wide spectral range can provide a perfect knowledge of atmospheric influence on astronomical observations. If the opacity measurements are done in a narrow (a few MHz) spectral coverage, it is impossible to distinguish between clear sky opacity, hydrometeors contributions, and systematic errors. A wide frequency coverage (several hundreds of GHz) is necessary to make sure we are in clear sky conditions and no instrumental offset is affecting our measurement and our analysis. In this way it is also possible to determine the dry and the wet continuum terms, see Pardo et al. (2001b).

A large spectral sampling can be achieved at the price of a bit complex instrument. The possibility to monitor the atmosphere towards different positions in the sky, also avoids bias due to a spatial model assuming the multi layers approximation.

A dedicated spectrometer, like the one proposed for Dome C (De Petris et al. (2005)) and in operation at Testa Grigia station (3500 m a.s.l., Alps, Italy) in a spectrally limited version (100 ÷ 360 GHz), CASPER 2 (Decina et al. (2010) and De Petris et al. *in prep.*), is a viable solution.

ACKNOWLEDGMENTS

We acknowledge Andrea Pellegrini and Paolo Grigioni for supplying us the radiosounding data and information obtained from IPEV/PNRA Project 'Routine Meteorological Observation at Station Concordia - www.climantartide.it' and Daniela Galilei for contributing to the preliminary radiosoundings data analysis.

APPENDIX A: CORRECTION OF THE RADIOSONDE DATA AND CALCULATIONS OF PRECIPITABLE WATER VAPOUR.

The meteorological data were obtained at Dome C using two Vaisala radiosonde models: (i) the RS92 model for 430 measurement days, i.e. for 94 per cent of the overall days, and (ii) the RS80-A model for 29 radiosonde launches only. Each triplet of signals giving the measurements of P, T and RH at a certain level was sent by the transmitter onboard the radiosonde to the ground station every 2 s. Considering that the radiosonde ascent rate was in general 5 - 6 m s^{-1}, the triplets of signals were recorded in altitude steps of 10 - 12 m.

The main characteristics of the three sensors (Barocap, Thermocap, and Humicap) mounted on the two radiosonde models are available in Table 1 of Tomasi et al. (2006), where their measurement range, resolution, accuracy, repeatability in calibration, and reproducibility in sounding are given.

The measurements of P, T and RH provided by the radiosonde sensors were all corrected following the procedure defined by Tomasi et al. (2006), which consists of numerous steps adopted to minimize the errors due to:

(i) the not correct calibration of the Barocap sensors;

(ii) the effects caused by solar and infrared radiation heating, heat conduction and ventilation on the Thermocap sensors;

(iii) lag errors, ground-check errors, and dry biases of the Humicap sensors due to basic calibration model, chemical contamination, temperature dependence and sensor aging, corrected according to Wang et al. (2002).

This procedure substantially differs from that defined by Tomasi et al. (2011a) only in the parts regarding the correction of solar heating dry biases for both A- and H-Humicap sensors: (1) those of the A-Humicap sensor were corrected by Tomasi et al. (2006) using the algorithm of Turner et al. (2003), while Tomasi et al. (2011a) preferred to use the algorithm derived more recently by Cady-Pereira et al. (2008); and (2) those of the H-Humicap sensor were corrected by Tomasi et al. (2006) using the average correction factors proposed by Miloshevich et al. (2006) as a function of solar zenith angle, while Tomasi et al. (2011a) employed the pair of day-time and night-time correction algorithms of Miloshevich et al. (2009). A large part of the few percent discrepancies found in the comparison shown in Fig. 3 between the present values of *pwv* and those determined by Tomasi et al. (2011a) arise from the use of these different algorithms in correcting the instrumental and solar heating dry biases affecting the field measurements of RH.

Using the correction procedures previously described, the daily vertical profiles of pressure $P(z)$, temperature $T(z)$ and $RH(z)$ were determined at fixed levels above the surface-level, in regular steps of 25 m from 3.25 to 4 km, 50 m from 4 to 5 km, and 100 m from 5 to 8 km amsl.

In order to calculate the values of absolute humidity $q(z)$ at the same fixed levels, the following procedure was adopted, consisting of the three steps: (i) calculation at each level of the saturation vapour pressure $E(T)$ in the pure phase over a plane surface of pure water, using the well-known Bolton (1980) formula; (ii) calculation at each level of the water vapour partial pressure $e(z)$ as the product $E(T) \times RH(z)$; (iii) calculation at each level of absolute humidity $q(z)$ (measured in $g\ m^{-3}$) in terms of the well-known equation of state of water vapour, and, hence, as the ratio between $e(z)$ (in hPa) and the product $R_w \times T(z)$ (in K), in which the water vapour gas constant $R_w = 0.4615\ J\ g^{-1}\ K^{-1}$ is put in place of the constant $R_a = 0.287\ J\ g^{-1}\ K^{-1}$ used in the equation of state for dry air.

For all the 469 daily vertical profiles of $q(z)$ obtained using the above procedure, the values of *pwv* were then calculated by integrating each vertical profile of $q(z)$ from the surface-level to 8 km amsl (i.e. up to 4.767 km above the ground level).

REFERENCES

Battistelli E. S. et al., 2012, MNRAS accepted for publication arXiv1203.5615

Bolton D., 1980, Monthly Weather Review, 108, 1046

Cady-Pereira K. E., Shephard M. W., Turner D. D., Mlawer E. J., Clough S. A., Wagner T. J., 2008, Journal of Atmospheric and Oceanic Technology, 25, 873

Calisse P. G., Ashley M. C. B., Burton M. G., Phillips M. A., Storey J. W. V., Radford S. J. E., Peterson J. B., 2004, PASA, 21, 256

De Petris M. et al., 2005, in EAS Publications Series, Vol. 14, EAS Publications Series, M. Giard, F. Casoli, & F. Paletou, ed., pp. 233–238

De Petris M. et al., 2002, ApJ, 574, L119

Decina B., De Gregori S., De Petris M., Lamagna L., 2010, in EAS Publications Series, Vol. 40, EAS Publications Series, L. Spinoglio & N. Epchtein, ed., pp. 107–110

Dempsey J. T., Friberg P., Jenness T., Bintley D., Holland W. S., 2010, in Society of Photo-Optical Instrumentation Engineers (SPIE) Conference Series, Vol. 7741, Society of Photo-Optical Instrumentation Engineers (SPIE) Conference Series

Holland W. S. et al., 1999, MNRAS, 303, 659

Lawrence J. S., 2004, PASP, 116, 482

Miloshevich L. M., Vömel H., Whiteman D. N., Leblanc T., 2009, Journal of Geophysical Research (Atmospheres), 114, 11305

Miloshevich L. M., Vömel H., Whiteman D. N., Lesht B. M., Schmidlin F. J., Russo F., 2006, Journal of Geophysical Research (Atmospheres), 111, 9

Minier V. et al., 2008, in EAS Publications Series, Vol. 33, EAS Publications Series, H. Zinnecker, N. Epchtein, & H. Rauer, ed., pp. 21–40

Pardo J. R., Cernicharo J., Serabyn E., 2001a, IEEE Transactions on Antennas and Propagation, 49, 1683

Pardo J. R., Serabyn E., Cernicharo J., 2001b, J. Quant. Spec. Radiat. Transf., 68, 419

Peterson J. B., Radford S. J. E., Ade P. A. R., Chamberlin R. A., O'Kelly M. J., Peterson K. M., Schartman E., 2003, PASP, 115, 383
Schaffer K. K. et al., 2011, ApJ, 743, 90
Swetz D. S. et al., 2011, ApJS, 194, 41
Tomasi C., Petkov B., Benedetti E., Valenziano L., Vitale V., 2011a, Journal of Geophysical Research (Atmospheres), 116, 15304
Tomasi C. et al., 2006, Journal of Geophysical Research (Atmospheres), 111, 20305
Tomasi C., Petkov B., Dinelli B. M., Castelli E., Arnone E., Papandrea E., 2011b, Journal of Atmospheric and Solar-Terrestrial Physics, 73, 2237
Tremblin P. et al., 2011, A&A, 535, A112
Turner D. D., Lesht B. M., Clough S. A., Liljegren J. C., Revercomb H. E., Tobin D. C., 2003, Journal of Atmospheric and Oceanic Technology, 20, 117
Valenziano L., Dall'Oglio G., 1999, PASA, 16, 167
Wang J., Cole H. L., Carlson D. J., Miller E. R., Beierle K., Paukkunen A., Laine T. K., 2002, Journal of Atmospheric and Oceanic Technology, 19, 981
Ward-Thompson D. et al., 2005, MNRAS, 364, 843
Yang H. et al., 2010, PASP, 122, 490